



**HAL**  
open science

## Ratiometric, single-dye, pH-sensitive inhibited laser-induced fluorescence for the characterization of mixing and mass transfer

Tom Lacassagne, Serge Simoens, Mahmoud El Hajem, Jean-Yves Champagne

► **To cite this version:**

Tom Lacassagne, Serge Simoens, Mahmoud El Hajem, Jean-Yves Champagne. Ratiometric, single-dye, pH-sensitive inhibited laser-induced fluorescence for the characterization of mixing and mass transfer. *Experiments in Fluids*, 2018, 59, pp.21. 10.1007/s00348-017-2475-y . hal-02085880

**HAL Id: hal-02085880**

**<https://hal.science/hal-02085880>**

Submitted on 19 Nov 2021

**HAL** is a multi-disciplinary open access archive for the deposit and dissemination of scientific research documents, whether they are published or not. The documents may come from teaching and research institutions in France or abroad, or from public or private research centers.

L'archive ouverte pluridisciplinaire **HAL**, est destinée au dépôt et à la diffusion de documents scientifiques de niveau recherche, publiés ou non, émanant des établissements d'enseignement et de recherche français ou étrangers, des laboratoires publics ou privés.

# Ratiometric, single dye, pH sensitive inhibited laser-induced fluorescence for the characterization of mixing and mass transfer

Tom Lacassagne · Serge Simoëns · Mahmoud El Hajem · Jean-Yves Champagne

Received: 21 September 2017 / Accepted: 9 December 2017

**Abstract** Inhibited Planar Laser Induced Fluorescence ( $I - PLIF$ ) techniques are widely used for heat and mass transfer studies in fluid mechanics. They allow the visualization of instantaneous two-dimensional field of a passive or reactive scalar, providing that this scalar acts as an inhibitor to the fluorescence of a specific molecule, and that this molecule is homogeneously mixed in the fluid at a known concentration. Local scalar values are deduced from fluorescence recordings thanks to preliminary calibration procedure. When confronted with non-optically thin systems however, the knowledge of the excitation intensity distribution in the region of interest is also required, and this information is most of the time hard to obtain. To overcome that problem, two-color ratiometric PLIF techniques ( $I^r - PLIF$ ) have been developed. In these methods, the ratio of two different fluorescence wavelengths triggered by the same excitation is used as an indicator of the scalar value. Such techniques have been used for temperature measurements in several studies but never, to the author's knowledge, for pH tracking and acid-base mixing, despite the frequent use of the one-color version in mass transfer studies. In the present work, a ratiometric pH sensitive inhibited PLIF technique ( $I_{pH}^r - PLIF$ ) using fluorescein sodium as a single dye and applicable to complex geometries and flows is developed.

Theoretical considerations show that the ratio of the two colors' fluorescence intensities should only depend on the dye's spectral quantum yield, itself pH dependent. A detailed spectrofluorimetric study of fluorescein reveals that this ratio strictly increases with the pH for two well-chosen spectral bands (fluorescence colors). A similar trend is found when using sCmos cameras equipped with optical filters to record fluorescence signals. The method is then experimented on a test flow, a turbulent acidic jet injected in an initially pH-neutral volume of fluid.

The results obtained using the ratiometric version are consistent with single color technique measurements, but excitation intensity heterogeneity is more efficiently accounted for, with a much smaller time needed for data treatment and without requiring the knowledge of laser paths across the fluid.

This new technique is also able to reduce the impact of some unwanted experimental features such as time varying excitation intensity or reflections at interfaces. It can be of great interest for further applications to multiphase mass transfer studies.

**Keywords** Fluorescence · pH · Ratiometric · PLIF · Turbulent mixing · Concentration measurement

## Nomenclature

|                 |  |
|-----------------|--|
| $(\cdot)_{rms}$ | Root Mean Square (RMS) operator          |
| $[\cdot]$       | Molar concentration                      |
| $\delta I_1$    | Intensity collected from spectral band 1 |
| $\delta I_2$    | Intensity collected from spectral band 2 |
| $\epsilon$      | Fluorescein molar extinction coefficient |
| $\lambda_e$     | Laser excitation wavelength              |
| $\lambda_f$     | (fluorescence) Wavelength                |
| $\bar{\cdot}$   | Temporal averaging                       |

Tom Lacassagne  
E-mail: tom.lacassagne@gmail.com

Serge Simoëns  
E-mail: serge.simoens@ec-lyon.fr

Univ Lyon, INSA de Lyon, Ecole Centrale de Lyon, Université Lyon 1, CNRS, LMFA UMR 5509, 69621 Villeurbanne Cedex, France

|                |  |
|----------------|--|
| $\phi$         | Fluorescence quantum yield                                   |
| $\tau_L$       | Turbulence integral timescale                                |
| $A$            | Optical constant   |
| $C$            | Fluorescent dye concentration                                |
| $C_A$          | Acid concentration   |
| $C_{A,\infty}$ | Bulk acid concentration                                      |
| $C_{A,inj}$    | Injection acid concentration                                 |
| $D$            | Nozzle diameter  |
| $dI_a$         | Local absorbed intensity                                     |
| $dI_f$         | Local fluoresced intensity                                   |
| $dt$           | Camera's exposure time                                       |
| $e_L$          | Laser sheet thickness  |
| $f$            | Lens focal length  |
| $f_r$          | Camera recording frequency                                   |
| $I_0$          | Laser output intensity                                       |
| $I_f$          | Fluoresced intensity   |
| $I_i$          | Incident intensity   |
| $I_r$          | Received fluoresced light intensity                          |
| $L_s$          | Length of fluid sample crossed by the incident beam          |
| $L_{obs}$      | Distance between a point in the fluid and the sensor         |
| $m$            | Mass of dissolved fluorescein                                |
| $Q$            | Jet flow rate  |
| $R$            | Spectral bands ratio   |
| $R^*$          | Wavelengths ratio  |
| $R_n$          | Normalized intensity ratio                                   |
| $R_r$          | Ratio submitted to re-absorption                             |
| $Re$           | Jet Reynolds number  |
| $S_\phi$       | Spectral quantum yield                                       |
| $s_{px}$       | Surface of the laser sheet corresponding to one camera pixel |
| $T$            | Temperature  |
| $U$            | Jet velocity   |
| $V_0$          | Main tank volume   |
| $V_1$          | Acid tank volume   |
| $V_2$          | Reservoir volume   |
| $V_s$          | Sample volume  |

## 1 Introduction and background

### 1.1 Introduction

Mass transfer at two-phase interfaces is of great interest in many applications in industrial, biological or environmental fields, but many of its aspects are still poorly understood, especially in presence of turbulent flows for liquid and/or gas phases.

The present work was motivated by two applications: the study of dissolution of atmospheric gases into water in presence of turbulence, which plays a key role in the understanding of sea water acidification (Turney and Banerjee 2013) or in the improvement of micro-alga

culture efficiency (Valiorgue et al 2014); and the investigation of gas dissolution and mixing in non-Newtonian fluids for chemical (Sossa-Echeverria and Taghipour 2012), pharmaceutical (Brujan 2010), or biological processes (Kawase et al 1987). For all of these fields of research, a better insight into the physics of turbulent reactive mixing close to gas-liquid interfaces is needed to improve numerical models.

The development of optical techniques such as Particle Image Velocimetry (PIV) or Laser Induced Fluorescence (LIF) since the end of the 1980's has increased the understanding of such phenomena. Indeed, those methods are non intrusive and can offer quantitative instantaneous data at multiple locations allowing the direct visualization of scalar transport and mixing in stationary or instationary flows. The main limitations are that the fluid has to be transparent and the mixing zone optically accessible.

In particular, Planar Laser Induced Fluorescence (PLIF) is of great interest, since it enables the direct measurement of a passive scalar value at a high spatial resolution and quick response time and even further micromixing measurement. Its principle is explained hereinafter.

A thin laser sheet is dispersed through a region of the studied flow. The fluid is seeded with a fluorescent molecule which has an absorption peak close to the laser excitation wavelength. The measurement of the dye's fluoresced light intensity leads to the quantitative determination of its concentration  $C$  thanks to a linear relationship between  $C$  and the fluoresced light intensity. This relationship stays linear only if the laser excitation intensity remains in the weak excitation regime (Chaze et al 2016; Simoens and Ayrault 1994). Using a multi-pixel light sensitive sensors (CMOS or CCD), one can record the fluorescence signal and thus determine the corresponding instantaneous concentration field.

For some fluorescent dyes, the emission intensity may also depend on the local value of a scalar characteristic of the flow. This makes it possible to deduce directly the value of this scalar from fluoresced light intensity measurement when the dye is homogeneously pre-mixed in the fluid at fixed concentration. Such techniques will hereinafter be referred to as  $I_i - PLIF$  as they are versions of PLIF where inhibition by species or scalar  $i$  occurs. For example, Rhodamine's thermal sensitivity can be used for temperature measurements ( $I_T - PLIF$ ) in different types of flows (Coolen et al 1999; Crimaldi 2008; Sakakibara et al 1997). The dissolved concentration of oxygen into water also tends to inhibit the fluorescence of Ruthenium with a Stern-Volmer type quenching law, as used by Jimenez (2013),

Butler et al (2016), Xu et al (2017) or Roudet et al (2017). This variation could be called  $I_{O_2} - PLIF$ .

## 1.2 $I_{pH} - PLIF$

In 1987, Walker (1987) proposed a technique equivalent to  $I_T - PLIF$  to measure punctually the pH value in acid/base reactive flows. His method is based on the pH dependency of the fluorescence of a family of dyes called fluoresceins, characterized by Lindqvist (1960) and Martin and Lindqvist (1975) (see part 2.1).

His work was used as a base for further development of pH sensitive Inhibited Planar Laser Induced Fluorescence ( $I_{pH} - PLIF$ ) and its application to the measurement of the dissolution of carbon dioxide around bubbles (Kuhn and Jensen 2012; Valiorgue et al 2013) or at flat surfaces (Asher and Litchendorf 2008; Lacasagne et al 2017; Variano and Cowen 2013). Indeed, it is well known that the dissolution of gaseous carbon dioxide into water results in the decomposition of the dissolved gas into carbonic acid. Carbonic acid reacts with water through two successive acid/base reactions to form sodium carbonate, bicarbonate, and protons, hence decreasing the pH (Stumm and Morgan 1996). Providing that these reactions' kinetics are fast enough (Asher and Litchendorf 2008; Valiorgue et al 2013), it is possible to access an instantaneous 2 dimensional dissolved gas concentration field thanks to  $I_{pH} - PLIF$ . The accuracy of this method is nevertheless limited by three main factors:

**Interfaces:** In presence of a moving interface such as a bubble or a free surface, laser reflections on this interface may result in heterogeneous and time-variable excitation intensity distribution in the laser sheet. If this distribution varies during the measurement, it becomes impossible to account for its heterogeneity simply using a reference image.

**Variations of excitation intensity field:** When confronted to non optically thin geometries, the absorption of the laser intensity on its path to the region of interest across the fluid becomes non negligible. If the area submitted to pH variation is small, this attenuation can easily be accounted for by using a reference image at a constant pH to correct Beer-Lambert absorption (keeping in mind the limitations denoted above). This is the case of figure 1 a.

**pH dependency of molar extinction coefficient:** The main issue is that fluorescein's molar extinction coefficient  $\epsilon$  depends on the pH. So if the area submitted to pH variations is large, the overall variations of molar extinction coefficient due to the pH may

become important. The intensity of excitation light reaching any point of the region of interest becomes function of the molar extinction coefficients encountered by the laser beam on its path, hence of the pH field, as in figure 1 b and c. It is assumed that the molar extinction coefficient is equivalent to a molar absorption coefficient, namely that all light attenuation comes from absorption by dye molecules. No other attenuation source exists (presence of particles ...). Valiorgue et al (2013) developed a correction procedure to overcome this effect, later completed by Souzy (2014). The principle introduced by Valiorgue is to record a series of images at different homogeneous pH before the measurement, and to build a specific calibration relation between intensity and pH for each pixel of the recorded image. The variations of excitation intensity due to the global pH variation with time are therefore taken into account. To tackle the issue of local pH heterogeneity, Souzy 2014 proposes to compute the value of the molar extinction coefficient of pixel columns  $n$  from the pH value at column of pixel  $n - 1$  for all images acquired during the measurements (figure 1). Scanning images from the column of pixel closer to the laser  $n_0$  to the furthest, and using the "pixel-by-pixel" calibration of Valiorgue, the pH and  $\epsilon$  field accounting for extinction coefficient variations on the laser path are simultaneously obtained.

This last procedure still presents some flaws. First the region of interest (ROI) has to be larger or equal to the region of the flow submitted to pH variation (ROV), otherwise the first column of pixel can't even be used as a reference since its pH is not known. Second, the step-by-step computation of pH and  $\epsilon$  introduces a cumulative error that could become important for the last columns of pixel treated. A last problem is the necessity to know the complete beam's path through the flow, which can only be achieved to the cost of spatial resolution.

This pixel-by-pixel calibration is also very long when treating several acquired images of fluorescence fields, since each pixel has to be calibrated and treated individually. To the authors' knowledge, very few people apart from Valiorgue have preferred the accuracy of the calibration over the time needed for treatment (Kuhn and Jensen 2012). Most of the time a compromise between spatial resolution and processing time is made by averaging the intensity values over groups of pixels before calibration and treatment.

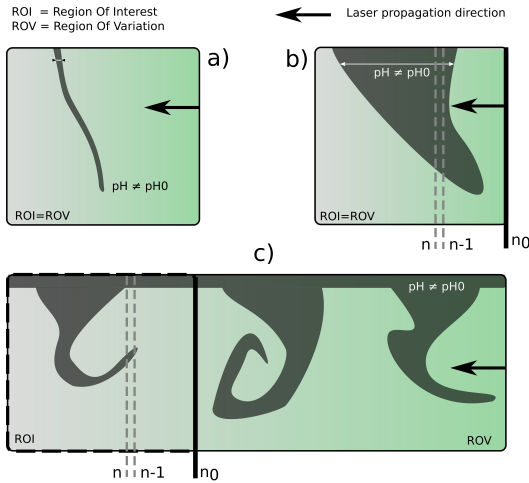


Fig. 1: Configurations of high laser attenuation a) easily correctable b) Correctable using a pixel-by-pixel method (Souzy 2014), c) Non correctable with a single color technique

### 1.3 Ratiometric developments and $I_T^r - PLIF$

To overcome the limitations stated above for non optically thin systems, an improvement of  $I - PLIF$  has been developed by Coppeta and Rogers (1998). The principle of this so-called "two-color" or ratiometric inhibited PLIF (later denoted as  $I_i^r - PLIF$  for inhibition by species  $i$ ) is to collect the fluorescent light emitted at two different wavelengths by a single dye or a pair of fluorescent dyes excited by the same laser. One wavelength is chosen such that its fluoresced light intensity strongly depends on the scalar quantity to measure, and the other one so that it does not. Dividing the first wavelength intensity field by the second one, the effects of heterogeneous or scalar-dependent excitation intensity mapping are corrected, since the excitation intensity is common to both fluoresced wavelengths. The two wavelengths may come from two different dyes, in which case the  $I_T^r - PLIF$  may be defined as "two colors - two dyes" (2c/2d) (Chaze et al 2016; Natrajan and Christensen 2009; Sakakibara and Adrian 1999), or from the spectrum of a single one, in which case one speaks of "two colors - one dye" method (2c/1d) (Bruchhausen et al 2005; Coolen et al 1999).

Since all fluorescence wavelengths collected come from the same excitation intensity, this last quantity does not impact the ratio of measured intensities, and only the dye concentrations and the targeted scalar characteristic do. The ratiometric procedure can consequently easily account for any temporal power drift of pulsed or Continuous Wave Lasers (CWL) during measurements, or for heterogeneous and time variable

distribution of excitation intensity in the laser sheet and the region of interest.

In two dyes systems, it is possible to measure relatively high fluoresced light intensity signals for both scalar sensitive and insensitive wavelengths. The major difficulty is to find a pair of dyes excitable by the same laser wavelength, and with a minimal spectral overlap between them to avoid spectral conflicts, as explained later. The measured ratio of fluorescence intensities also depends on the ratio of the two dyes concentrations, that needs to be exactly known and remain constant everywhere in the fluid during the experiment. For example, when confronted to turbulent flows, it must be assumed that the two dyes diffuse similarly (Lavieille et al 2004). On the other hand, single dye methods may be easier to implement since they only require to know the absorption and fluorescence spectra and the concentration of a single fluorescent compound. They are also less chemically intrusive since they only require the addition of one chemical component instead of two inside the fluid. But as for two dyes systems, the dye has to be wisely chosen to avoid spectral conflicts.

Spectral conflicts are due to overlaps between absorption and/or fluorescence spectra of one or several dyes. They have been classified in three main categories (Chaze et al 2016; Coppeta and Rogers 1998), sketched in figure 2:

- **Type I** conflicts are specific to two dyes systems and arise when the two fluorescence spectra of the two selected dyes partially overlap, so that some of the fluorescence of one dye can be wrongly interpreted as coming from the other dye. Sakakibara and Adrian (1999) addressed this situation in the context of temperature sensitive measurements and showed that this strongly reduces the accuracy of measurements.
- **Type II** conflicts are due to an interference between the absorption spectrum of one dye and the fluorescence of the same or the other dye. They are therefore not limited to two dyes systems, but extend to single dye systems where the Stokes shift is small (wavelength lag between the absorption and the emission peaks of a fluorescent molecule as sketched one figure 2). In that case, part of the fluoresced light intensity emitted is reabsorbed, and the fluoresced light intensity measured by the sensor becomes dependent on the length of fluid crossed by the fluorescence signal to reach it. Such effect can be neglected if this path is short enough (see section 2.2). If this is not the case, it can be corrected using a reference fluorescence ratio image to normalize the

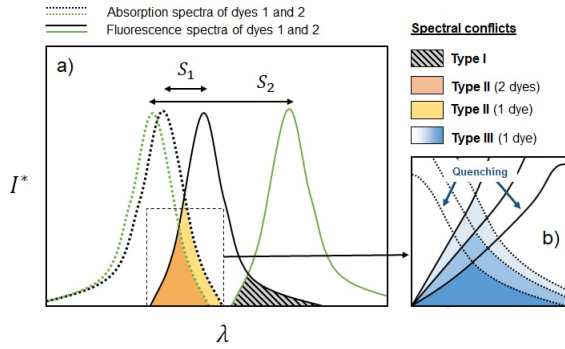


Fig. 2: Illustration of the different types of spectral conflicts. Type I and type II for one and two dyes configurations (a), and example of type III for one dye configuration (b).  $S_1$  and  $S_2$  are the Stokes shifts of dye 1 and 2 respectively

measured intensities, inasmuch as the spectral overlapping does not depend on the scalar quantity to be measured. A three-color method can also be used to corrects the adverse effect that reabsorption does not affect to the same extent all the wavelengths within a detection band (Lavieille et al 2004).

- If the spectral overlapping area depends on the measured scalar, type II conflicts becomes a **type III** one (figure 2b). The intensity collected by the sensor is not only dependent on the path length of the fluorescence signal between the laser sheet and the light collection device, but also on the scalar values encountered by the fluoresced light emission signal on its way to the sensor. If this path length or the dye concentration are too important for fluorescence reabsorption phenomena to be neglected (see section 4.2), this conflict can not be corrected by ratiometric methods (2c/2d or 2c/1d).

Since the proof of concept of the ratiometric methodology made by Coppeta and Rogers (1998) for both temperature and pH measurements, the temperature sensitive version has been regularly improved (Bruchhausen et al 2005; Chaze et al 2016; Coolen et al 1999; Lavieille et al 2004; Natrajan and Christensen 2009; Sakakibara and Adrian 1999). The pH sensitive ratiometric PLIF (hereinafter referred to as  $I_{pH}^r - PLIF$ ) has been mainly used in its two dyes version (2c/2d) for pH measurement in macromixing and micromixing studies and two-phase flows mass transfer (Kováts et al 2017; Lehwald et al 2010). In particular, Kováts et al (2017) show that bubble shadows and laser sheet heterogeneity can be reduced drastically by using a 2 color technique for pH measurement. Yet, the corrective potential of the ratiometric method has never been fully investigated. Other uses of ratiometric fluo-

rescence pH measurement can be found in the field of health science, e.g. in cellular biology as a mean of visualizing and understanding cellular processes (Bassnett et al 1990; Buckler and Vaughan-Jones 1990; Morris 1990), or in ophthalmology (Doughty 2014).

The present paper aims at applying the "two colors - one dye" (2c/1d) methodology developed for thermometry (Bruchhausen et al 2005) to the pH measurement inside aqueous turbulent flows. A single dye system is chosen over a two dyes one in order to keep the method as simple to implement and as weakly chemically intrusive as possible. The method will hereinafter be called "two color" or ratiometric, without specifying that it is a "single dye" version. The pH sensitivity of fluorescein sodium fluorescence spectrum is used to build a pH dependent ratio between two selected spectral bands. The theoretical expression of this ratio as a function of pH is derived in section 2, and investigated by a spectrofluorimetric study in section 3. Section 4 presents an application of the method to the visualization of acid/base mixing in a monophasic turbulent jet.

## 2 Theory of $I_{pH}^r - PLIF$

### 2.1 Fluorescein sodium

Fluoresceins are fluorescent molecules used in many scientific domains thanks to their high water solubility, high fluorescence quantum yield, and high sensitivity to several physico-chemical parameters like temperature or pH. They can be found for example in medical applications (*in-vivo* drug tracking, tumor targeting...) and are among the most common fluorescent dyes used in PLIF application. A wide variety of fluoresceins exists. The one used here is fluorescein disodium salt, also called fluorescein sodium, and has been purchased at Alfa Aesar.

Stable at solid state in the form of a red-orange powder, it has the ability to emit fluorescence radiation. Its spectrum is centered around the wavelength  $\lambda_f = 515 \text{ nm}$  when excited by a  $\lambda_e = 488 \text{ nm}$  incident wavelength. Its experimental spectrum is presented in section 3 figure 7. In fact, once dissolved into water, fluorescein decomposes into several forms through a rather complex set of polytropic equilibria. These have been studied by Martin and Lindqvist (1975) who have shown that 9 forms of fluorescein exist and can be classified into 4 categories: cations  $Fl^+$ , neutral forms  $Fl^0$ , anions  $Fl^-$  and dianions  $Fl^{2-}$ . For the needs of this study, the acid/base equilibria of fluorescein sodium dissolved in water have been numerically solved using Matlab, and the Bjerrum plot (concentration of each form

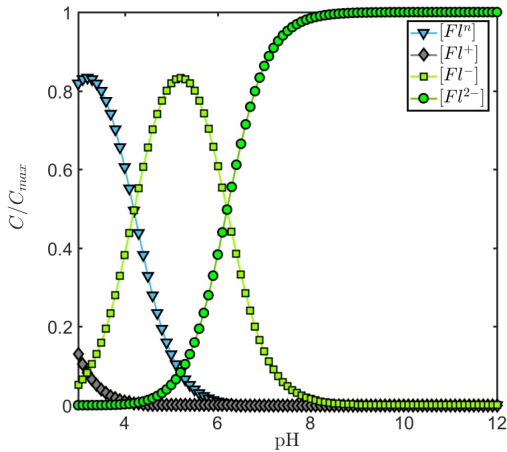


Fig. 3: Bjerrum plots of fluorescein sodium system

divided by total product concentration) of the four categories' concentrations as a function of pH are plotted in figure 3, where  $[X]$  denotes the molar concentration of species  $X$ .

Each of these species plays its own role in the absorption and emission processes, having its own molecular extinction coefficient  $\epsilon$  and its own quantum yield  $\phi$  (Guilbault 1990). It has also been shown that among all the possible forms, only the anionic ones have the ability to fluoresce.

Experimental curves of fluoresced light intensity or molar extinction coefficients as a function of pH have been plotted by Martin and Lindqvist (1975) and Walker (1987). They showed that relative fluoresced light intensity or relative extinction coefficient reaches its plateau value around pH 8, and that the maximum pH sensitivity lays between pH 5 and 8. It corresponds well to the variations of acidity that could be caused by  $CO_2$  dissolution and therefore makes it an efficient tracer for its absorption into water for example.

This behavior can be understood using a simple approach based on the proportion of fluorescent forms of fluorescein. The computation of  $[Fl^-] + [Fl^{2-}]$  with the same Matlab program that has been used before gives us the trend drawn in figure 4 for the sum of the fluorescent species' concentration as a function of pH. A theoretical computation of  $\epsilon$  for  $\lambda_e = 491 \text{ nm}$  can be made using the corresponding values of all extinction coefficients determined by Klonis and Sawyer (1996) reported in table 1 and a simple mixing law to estimate a total extinction coefficient.

$$\epsilon(\lambda_e, pH) = \sum_{i=1}^N \epsilon^i(\lambda_e) \cdot [Fl^i](pH) \quad (1)$$

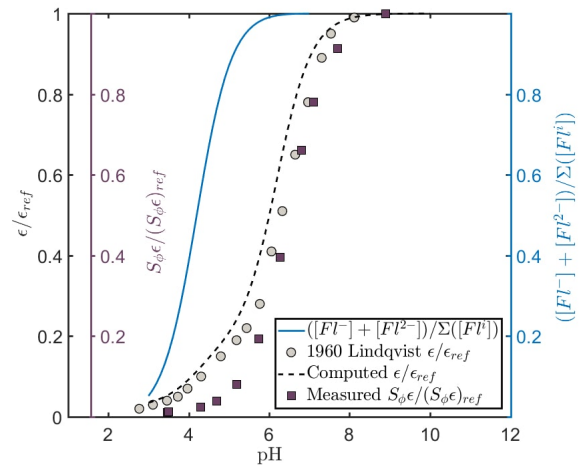


Fig. 4: Evolution of the normalized molar extinction coefficient at  $\lambda_e = 491 \text{ nm}$  computed from the values of table 1 using matlab (dashed line), and measured by Lindqvist (1960) (circles). The full line is the concentration of fluorescent species normalized by total fluorescein concentration. Square markers show the normalized excitation spectrum intensity values  $\frac{S_\phi(\lambda_f, pH)\epsilon(\lambda_e, pH)}{S_\phi(\lambda_f, pH_{ref})\epsilon(\lambda_e, pH_{ref})}$  measured for  $\lambda_f = 513 \text{ nm}$  at  $\lambda_e = 491 \text{ nm}$  (see section 3 for measurements and 2.3 for a definition of  $S_\phi$ )

| Fluorescein form | $\epsilon \text{ (} M^{-1} \cdot \text{cm}^{-1} \text{)}$ |
|------------------|---|
| $Fl^+$           | 30  |
| $Fl^n$           | 2700  |
| $Fl^-$           | 16000   |
| $Fl^{2-}$        | 88000   |

Table 1: Extinction coefficient values at  $\lambda = 491 \text{ nm}$  from Klonis and Sawyer (1996)

The same reasoning can be made for fluorescence quantum yield:

$$\phi(pH) = \sum_{i=1}^N \phi_i \cdot [Fl_i](pH) \quad (2)$$

With  $N = 4$ .

## 2.2 Equations for a single emission wavelength

For a given excitation wavelength  $\lambda_e$ , the incident intensity at point  $M$  of the fluid may be written according to Beer-Lambert absorption law as

$$I_i(M) = I_0 A \cdot e^{-\int_0^{L_s(M)} C(r)\epsilon(\lambda_e, pH(r))dr} \quad (3)$$

where  $I_0$  is the output laser intensity,  $A$  is a constant which depends on the optical setup used to format the

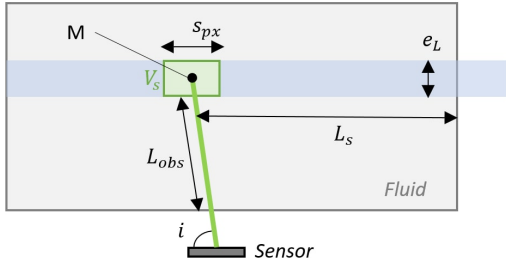


Fig. 5: Distances and parameters of the beams' paths (not to scale)

laser sheet,  $L_s(M)$  is the length crossed by a laser beam before reaching point  $M$ ,  $C(r)$  is the concentration of fluorescent dye in the fluid at any point and  $\epsilon$  the extinction coefficient of the dye. This last quantity varies inside the fluid since it depends on the local pH values.

During measurements, pH spatial variations make every pH dependent quantities spatially variable. In what follows, we will express these quantities as a function of the position  $M$ . To simplify the equations,  $\epsilon(pH(M))$  for example will be written as  $\epsilon(M)$ . As for  $C$  however, if the dye is perfectly mixed with the fluid prior to the experiments, it is itself independent of the location.

The absorbed incident intensity  $dI_a(M)$  at point  $M$  can then be expressed as

$$dI_a(M) = I_i(M)C\epsilon(\lambda_e, M)dV \quad (4)$$

and from equation 3

$$dI_a(M) = I_0AC\epsilon(\lambda_e, M).e^{-C \int_0^{L_s(M)} \epsilon(\lambda_e, r)dr} dV \quad (5)$$

and the fluoresced light intensity  $dI_f(M)$  emitted by this volume is

$$dI_f(M) = \phi(M).dI_a(M) \quad (6)$$

or, from equation (5)

$$dI_f(M) = I_0AC\phi(M)\epsilon(\lambda_e, M).e^{-C \int_0^{L_s(M)} \epsilon(\lambda_e, r)dr} dV \quad (7)$$

Equation (7) can be integrated over a small volume  $V_s$  centered around  $M$ , assuming that  $\epsilon$  at  $\lambda_e$  and  $\phi$  in  $V_s$  are constant within this volume.

$$I_f(M) = \int_{V_s} dI_f \quad (8)$$

and from equation 7 it comes that

$$I_f(M) = I_0AC\phi(M)\epsilon(\lambda_e, M)V_s.e^{-C \int_0^{L_s(M)} \epsilon(\lambda_e, r)dr} \quad (9)$$

Typically,  $V_s = s_{px}.e_L$  where  $e_L$  is the laser sheet thickness and  $s_{px}$  the surface of the area recorded on a single pixel of the sensor (see figure 5).

The fluoresced intensity  $I_r(M)$  reaching the sensor coming from point  $M$  is then

$$I_r(M) = I_f(M).e^{-C \int_0^{L_{obs}(M)} \epsilon(\lambda_f, r).dr} \quad (10)$$

where  $L_{obs}(M)$  is the distance traveled in the fluid by fluoresced light of wavelength  $\lambda_f$  emitted from point  $M$  before reaching the sensor.

The term  $e^{-C \int_0^{L_{obs}(M)} \epsilon(\lambda_f, r).dr}$ , represents the re-absorption of fluoresced light by the fluid, that can lead to type II or III spectral conflicts (see section 1). It can be neglected if  $C\epsilon L_{obs} \ll 1$  for all  $M$  of the observed region. This is a part of the "optically thin system" assumptions of Walker (1987). Typically for fluorescein sodium, the fluorescence extinction coefficient for  $\lambda = \lambda_f = 515 \text{ nm}$  is  $\epsilon \sim 10^4 \text{ M}^{-1}.\text{cm}^{-1}$  at  $pH > 12$  where it reaches its maximum (Klonis and Sawyer 1996; Martin and Lindqvist 1975). For the fluorescein sodium concentration used in the present study  $C = 5.10^{-7} \text{ M}$ ,  $L_{obs} \ll \frac{1}{\epsilon C} = 200 \text{ cm}$  is required to fulfill this condition.

If this is verified for the chosen  $\lambda_f$ ,  $I_r(M) \approx I_f(M)$  and so

$$I_r(M) \approx I_0ACV_s\phi(M).\epsilon(\lambda_e, M).e^{-C \int_0^{L_s(M)} \epsilon(\lambda_e, r)dr} \quad (11)$$

### 2.3 Equations for the ratio of two wavelengths or spectral bands

Considering now a polychromatic fluoresced light and not only a single emitted wavelength, equation (11) becomes

$$I_r(\lambda_f, M) \approx I_0ACV_s\epsilon(\lambda_e, M)S_\phi(\lambda_f, M).e^{-C \int_0^{L_s(M)} \epsilon(\lambda_e, r)dr} \quad (12)$$

$S_\phi$  may be seen as the "spectral" quantum yield of fluorescence, that is to say the amount of absorbed energy turned into fluorescence light at wavelength  $\lambda_f$ , with  $\phi(M) = \int_0^\infty S_\phi(\lambda_f, M)d\lambda_f$ .

Since only  $S_\phi$  depends on  $\lambda_f$ , the ratio  $R^*$  of the received intensity at two different fluoresced wavelengths  $\lambda_1$  and  $\lambda_2$  (see figure 6a) from the same given point  $M$  can simply be expressed from equation (12) as

$$R^*(\lambda_1, \lambda_2, M) = \frac{I_r(\lambda_1, M)}{I_r(\lambda_2, M)} = \frac{S_\phi(\lambda_1, M)}{S_\phi(\lambda_2, M)} \quad (13)$$

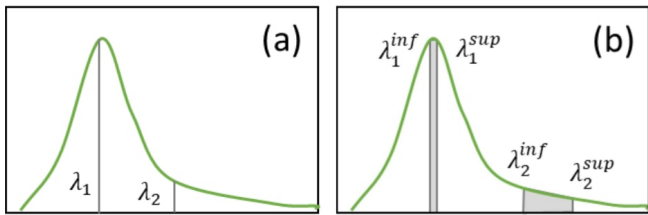


Fig. 6: Selection of fluorescence wavelengths (a) and spectral bands (b)

| Type of spectrum | $\lambda_e$ (nm) | $\lambda_f$ (nm) |
|------------------|------------------|------------------|
| Excitation       | 400 - 510        | 513              |
| Fluorescence     | 470              | 475 - 650        |
| Fluorescence     | 488              | 492 - 650        |

Table 2: Wavelengths used for the present spectral study

In the same way, the ratio  $R$  for fluoresced intensity integrated over two spectral bands (see figure 6b) is

$$R(\lambda_1^{inf}, \lambda_1^{sup}, \lambda_2^{inf}, \lambda_2^{sup}, M) = \frac{\int_{\lambda_1^{inf}}^{\lambda_1^{sup}} S_\phi(\lambda, M) d\lambda}{\int_{\lambda_2^{inf}}^{\lambda_2^{sup}} S_\phi(\lambda, M) d\lambda} \quad (14)$$

In both cases, one can see that for known fluorescence wavelengths, the ratio depends only on  $M$ , that is to say on the local value of the pH, which is precisely what is needed.

For the technique to be suitable for pH measurement, it has to be checked that this ratio is monotonous for the chosen spectral bands or wavelengths, and that its dynamic of variation is large enough to ensure a good sensitivity of measurement. This validation is the object of the spectrofluorimetric study presented in part 3.

### 3 Spectral study

#### 3.1 Measurements and data treatment

Fluorescence excitation and emission spectra have been plotted using an FLS90 Edinburgh Instruments spectrofluorimeter. Excitation spectra are obtained by measuring the fluoresced light intensity at a given wavelength  $\lambda_f$  for a range of excitation wavelengths  $\lambda_e$ . Fluorescence emission spectra are obtained measuring the fluoresced light intensity of different wavelengths  $\lambda$  for a given excitation wavelength  $\lambda_e$ . The wavelengths chosen for the present study are given in table 2.

The opening and exposure time of the spectrofluorimeter have been set so that its output signal at the

intensity peak of the most basic sample at the best excitation wavelength is close to its maximum voltage without being saturated. By that means, the best dynamical range is obtained and the error reduced, even for highly acidic samples yielding weak fluorescence signals.

The samples consist in fluorescein-sodium solutions at  $C = 5.10^{-7} M$ , the pH of which is set by two types of buffer solutions, sodium carbonate / sodium bicarbonate and citric acid / sodium phosphate, allowing for a pH variation between 3.5 and 10.3.

#### 3.2 Results

##### 3.2.1 pH and spectra

From figure 7 a, the pH dependency of fluorescein sodium behavior can clearly be seen. The fluoresced light intensity peak strongly decreases with acidity especially in the range between  $pH = 8$  and  $pH = 5$  but its position remains at  $\lambda_f = 515 nm$  (see figure 7 a and c). The dependency of the excitation spectrum on the pH can also be seen on the figure, but what differs from the fluorescence one is that the peak excitation wavelength varies when the pH becomes lower than 5.5 (7 a and b). The excitation peak at  $\lambda_e = 488 nm$  tends to decrease and an other excitation peak at  $\lambda_e = 437 nm$  appears.

This second peak corresponds to the absorption maximum wavelength for the neutral  $Fl^0$ , cationic  $Fl^+$  and monoanionic  $Fl^-$  forms of fluorescein, whereas 488 nm is the maximum absorption wavelength of the di-anionic form (Klonis and Sawyer 1996; Martin and Lindqvist 1975). Under monochromatic excitation of  $\lambda_e = 488 nm$ , the decrease in fluoresced light intensity can therefore be explained by two factors: the fact that the extinction coefficient is decreased with acidity, and the fact that 488 nm is no longer the preferred absorption wavelength when reaching acidic pHs. Let's take the example of absorption and fluorescence at pH 4: even if one of the two fluorescent forms,  $Fl^-$ , is still present (see Bjerrum plots in figure 3) and the total concentration of fluorescent species is still relatively high (see figure 4), the excitation of the single fluorescent form left is not optimal.

This feature will not be further addressed in the present paper, but it could be of great interest if one wants to extend the sensitivity of fluorescein-based  $I - PLIF$  techniques to acidic pHs. Using simultaneously  $\lambda_e = 488 nm$  and  $\lambda_e = 437 nm$  excitation, it would be possible to trigger both fluorescent forms of fluorescein at their optimal excitation intensity. As compared to the case of a single excitation wavelength, this could increase the level of fluoresced light intensity

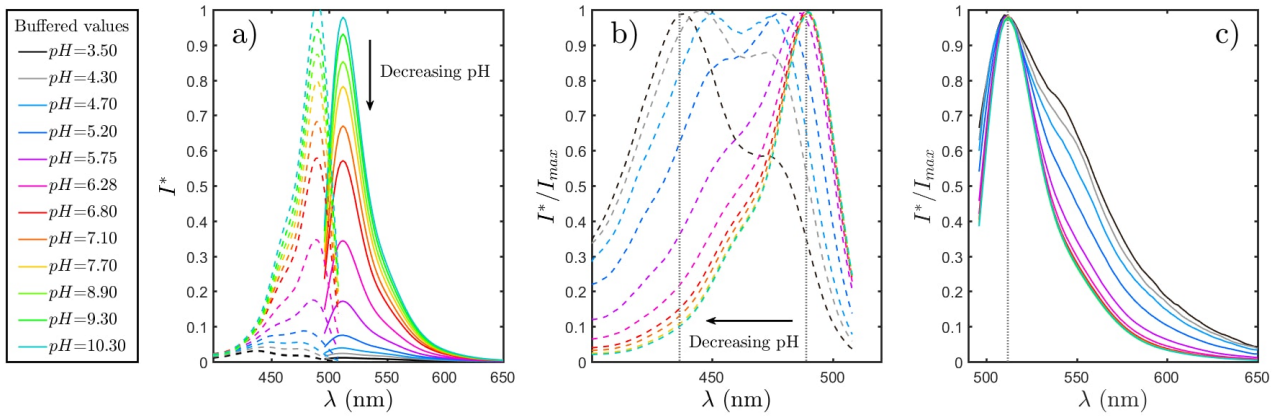


Fig. 7: Excitation (dashed lines) and fluorescence spectra (full lines) of  $C = 5.10^{-7} M$  fluorescein sodium solution as a function of pH (a) Raw spectra (arbitrary units) (b) Excitation spectra normalized by their maximum intensity (c) Fluorescence spectra normalized by their maximum intensity. Dotted lines mark the position of absorption and emission peaks.

especially in the pH range between 4 and 5 where  $Fl^-$  dominates (see figure 3), and extend the measurable intensity range, hence the sensitivity, to the low pH regions.

Finally, it can be seen in figure 7 that the two spectra overlap in the 490–510 nm region. The overlapping area increases with the pH, thus leading to a type III spectral conflict. When applying the method to cases where fluorescence re-absorption is not negligible, this could cause important errors. This point is addressed later on in section 4.

### 3.2.2 Proposition of two spectral bands

Based on the previous spectra it is clear that the best pH dependency dynamics for the fluorescence signal is found around the peak wavelength, and that the tail of the spectrum (wavelengths above 560 nm) is far less sensitive to pH variations. The ratio  $R^*$  defined in equation (13) for  $\lambda_1 = 515 nm$  and  $\lambda_2 > 560 nm$  should therefore be suitable to study pH variations.

Nevertheless, this ratio  $R^*$  of wavelengths is technically difficult to measure. Indeed, when using an optical setup to collect the fluoresced light and not a specifically designed spectrofluorimeter, the intensity level of wavelength  $\lambda_2$  has to be sufficiently above the measurement noise, which means that  $\lambda_2$  has to be close enough to the fluorescence peak. Moreover, separation of colors with such optical setups is done by optical filters placed in front of the recording cameras. Those filters select ranges of wavelengths and not discrete ones. It is therefore more convenient to use the expression of the

ratio  $R$  for spectral bands expressed in equation (14), and one has to check that the amount of light collected from spectral band 2 is high enough (figure 8).

The best compromise between dynamics of the  $R$  ratio, available optical filters, and intensity level collected from band 2 was found to be with  $\lambda_1^{inf} = 510 nm$ ,  $\lambda_1^{sup} = 520 nm$ ,  $\lambda_2^{inf} = 560 nm$  and  $\lambda_2^{sup} \rightarrow +\infty$ . This couple of spectral bands also presents the advantage of leaving the 532 nm neighborhood open (see figure 8). This is useful if one wants to couple the concentration measurements with PIV techniques using Nd:YAG pulsed laser emitting at 532 nm wavelengths (Lacassagne et al 2017).

The behavior of fluorescence emission at chosen spectral bands can be derived by numerically integrating the measured excitation spectra at different pHs. It is then easy to compute the ratio curve  $R = f(pH)$  (see figure 9).

For the two selected spectral bands indicated in figure 8, pH dependency of the integrated intensities  $\delta I_1$  and  $\delta I_2$  and of the ratio  $R$  are plotted in figure 9. Both intensities have the same S-shaped curve, reaching their maximum at pH around 9. As expected, the intensity variations of  $\delta I_2$  are lower than that of  $\delta I_1$ . The ratio  $R$  is strictly increasing over the whole pH range, and exhibits a good dynamics between pH 4 and 8, and a quasi-linear trend between pH 5 and 7. At acidic pH, integrated intensity over band 2 is larger than over band 1 since it is wider, hence the ratio is below 1. On the contrary, for basic pH, band 1 integrated intensity is much higher since it captures the fluorescence peak, which is no longer inhibited, hence the ratio is above 1. The whole curve can be fitted by an hyperbolic

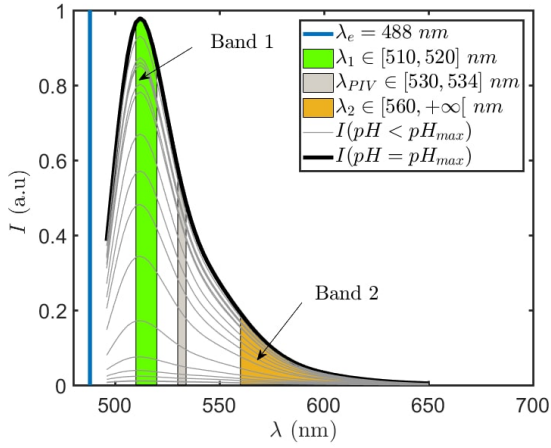


Fig. 8: Location of chosen spectral bands: band 1 in green and band 2 in orange. The gray stripe represents the spectral band admitted by optical filters generally used for PIV measurements (Lacassagne et al 2017). Excitation wavelength is represented by the blue vertical line. Black solid line is the fluorescence spectrum measured at the maximum fluoresced light intensity, dashed lines are spectra measured at lower pHs.

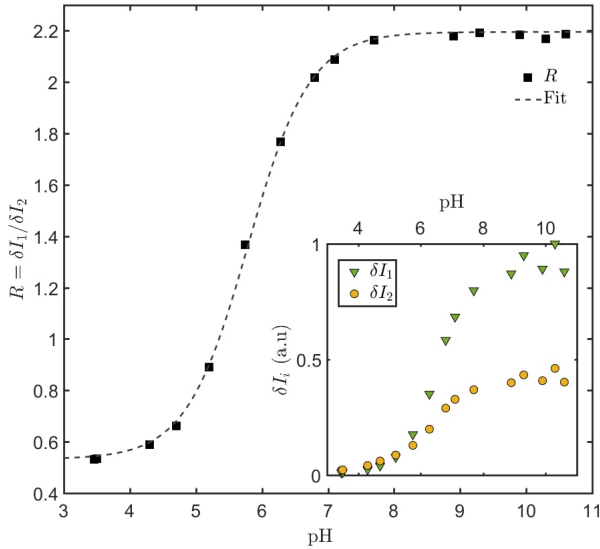


Fig. 9: Spectral band intensities and ratio as a function of pH measured by spectrofluorimetry. Main figure: Computed ratio and hyperbolic fitting, Insert: Spectral band intensities

tangent function, which is a reflection of the exponential behavior of chemical equilibria of the several forms of fluorescein responsible for quantum yield variations. Ratio points measured for a lower fluorescein sodium concentration (not presented here) also fit well to the same curve, hence fluorescein sodium concentration in

the  $[10^{-8} - 10^{-7}] M$  domain has no influence on the shape of the fluorescence spectrum.

These results therefore confirm the possible application of single dye  $I_{pH}^r - PLIF$  using fluorescein sodium, at least from the spectral point of view. For the proof of concept to be completed, a test case of turbulent monophasic pH mixing is proposed in the following section.

#### 4 Example of application: Mixing of an acidic jet into a basic medium

A monophasic turbulent round jet was used as a benchmark to test the  $I_{pH}^r - PLIF$  method. This type of flow has been widely studied in the literature (Papanicolaou and List 1988; Papantoniou and List 1989) and has been used as a test flow for the development of PLIF techniques by Walker (1987), Bruchhausen et al (2005) or Chaze et al (2016) for example. In this section, the calibration procedure is first addressed, and the case of an acidic jet immersed in a neutral solution is then studied. The pH fields given by the proposed method are compared to the ones obtained using single color  $I_{pH} - PLIF$  with different calibration procedures.

##### 4.1 Experimental setup

###### 4.1.1 Jet

The turbulent jet is created by a  $D = 1 mm$  nozzle placed inside a  $277 \times 277 \times 500 mm^3$  Plexiglas tank. About 100 L of fluorescein sodium solution at a given concentration  $C$  in water are prepared.  $V_0 = 40 L$  of it are placed inside the tank and  $V_1 = 20 L$  are placed in a secondary tank. Chlorhydric acid HCl is then added to the secondary tank to decrease its pH down to about 4.6. The acidic solution thus formed is injected in the main tank to generate the turbulent jet (figure 10). This first step allows the fluorescein concentrations of the jet and the receiving fluid to be rigorously identical, so that the fluoresced light intensity variations observed during the measurements can only be explained by pH variations. The remaining volume  $V_2$  of fluorescein solution is stored a reservoir and can be used to replace the acidified fluid of the main tank between two experiments. The pH inside tanks 1 and 2 are checked prior to the experiment using a Hanna Checker pH meter. Since HCl is a strong acid, the relationship between pH and concentration of transported scalar is  $pH = -\log(C_A)$  and the injection concentration is  $C_{A,inj} \simeq 2.10^{-5} M$ . Temperatures in both tanks are checked to be equal and remain

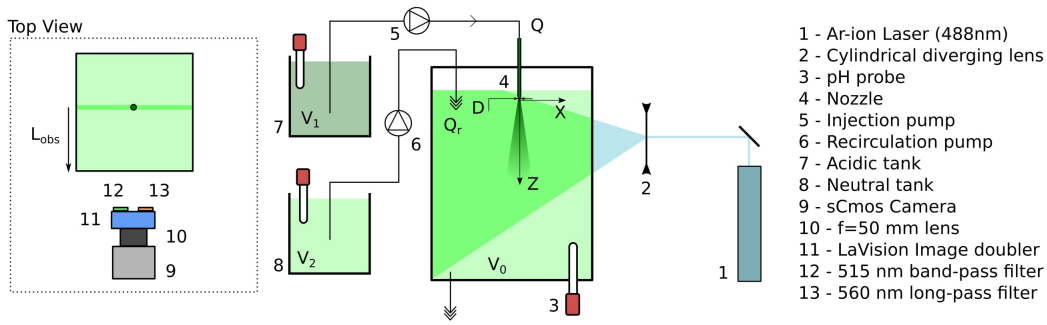


Fig. 10: Sketch of the setup designed for the turbulent jet experiment

constant during the whole experiment, so that the low temperature dependency of fluorescein's fluorescence doesn't influence the measurements.

A pump connected to tank 2 generates an injection flow rate of about  $Q \simeq 0.15 \text{ L.min}^{-1}$  which yields a velocity of about  $U \simeq 3 \text{ m.s}^{-1}$  and a jet Reynolds number  $Re = \frac{UD}{\nu} \simeq 3000$  at room temperature ( $T = 20^\circ\text{C}$ , fixed throughout the experiments). At this flow rate, the volume of acidic fluid injected during the time of measurement (typically 2 minutes) is less than 0.3 % of the initial volume of neutral fluid, which leads to a bulk concentration increase of  $10^{-7} \text{ M}$ . It can therefore be assumed that the bulk concentration  $C_{A,\infty}$  in the tank remains constant during the time of experiment.

#### 4.1.2 Optical setup

The jet region is illuminated by a  $\lambda_e = 488 \text{ nm}$  laser sheet of thickness  $e_L \simeq 1 \text{ mm}$  using a Stabilite 2017 Argon-Ion Continuous Wave Laser. The fluorescence spectral bands are separated using two optical filters, one band-pass of central wavelength  $515 \text{ nm}$  and bandwidth  $10 \text{ nm}$ , and one long-pass of cutoff wavelength  $560 \text{ nm}$ . Both filters are placed on a LaVision image doubler that allows the two fluorescence signal to be recorded on the same sensor. Here a LaVision sCmos camera is equipped with a  $f = 50 \text{ mm}$  lens. The pixel size is  $dx = dy = 0.1 \text{ mm/pixel}$ . The sampling volume  $V_s$  defined in section 2.2 is therefore  $V_s = dx \times dy \times e_L = 0.01 \text{ mm}^3$ . This quantifies the spatial resolution achievable by this setup. Intensities on measurement images reach up to 22000 gray levels for band 1 and 7000 gray levels for band 2. At the lowest measured pH, intensities are always above 1400 gray levels, much higher than the noise level (of about 400 gray levels).

#### 4.1.3 Data treatment

Each image is split into two sub-images corresponding to the two halves of the sensor recording each wavelength. A reference image of a test pattern is taken prior to the experiment to enable the separation of the two parts of the recorded image and their spatial correlation. The camera exposure time is set at  $dt = 20 \text{ ms}$  as a best compromise between the amount of fluorescence light collected on both parts of the sensor and the temporal resolution. The region of interest is cropped out, and the spatial correlation for each sub-image is found using the two sub-images extracted from the recorded test-pattern. Sub-image 2 of the test pattern is shifted and rotated over sub-image 1 in order to maximize the cross correlation between sub images 1 and 2. The same translation/rotation is then applied to every recorded image.

#### 4.1.4 Uncertainties

The relative uncertainty on ratio measurement can be expressed as

$$\frac{\Delta R}{R} = \frac{\Delta \delta I_1}{\delta I_1} + \frac{\Delta \delta I_2}{\delta I_2} \quad (15)$$

The maximum uncertainty corresponds to the lower pH values where both fluorescence emissions are minimal. With the optical setup used, one typically gets  $\delta I_1 \simeq 1400$  gray levels and  $\delta I_2 \simeq 2000$  gray levels for  $pH = 4.6$ . Considering a global uncertainty of  $\Delta \delta I_1 = \Delta \delta I_2 = 1$  gray level, the relative uncertainty on the ratio is  $\Delta R/R \sim 0.1 \%$  for  $pH = 4.6$  and falls to  $0.05 \%$  for  $pH = 7$ . The optical noise being of about 400 gray levels, the signal over noise ratio lays between about 4 for low pHs and 25 for high pHs.

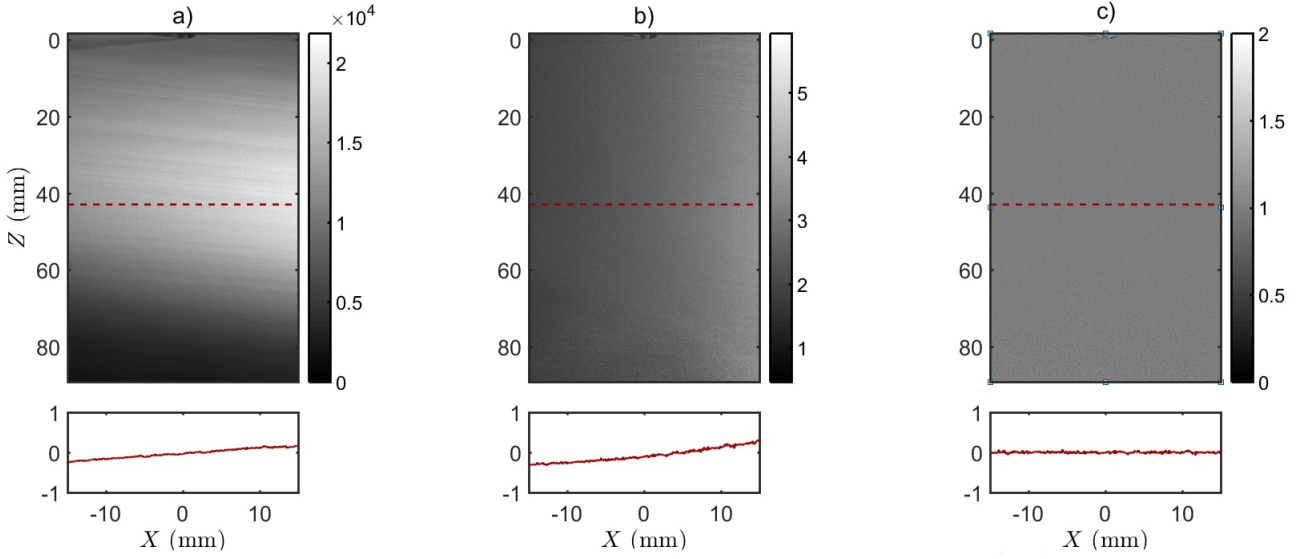


Fig. 11: Calibration images at homogeneous  $pH = 7$ , (a) is the raw intensity fluorescence for band 1 in arbitrary units, (b) is the raw ratio, and (c) is the normalized ratio. Horizontal variation profiles at  $Z = 43 \text{ mm}$  (dotted line) defined for each quantity  $i$  as  $(i - i_{ref})/i_{ref}$  are plotted under each field

#### 4.2 Calibration

The calibration procedure is performed by taking images of several solutions at homogeneous pH under constant laser excitation. The sub-images for each spectral band exhibit heterogeneous distribution of fluoresced light intensity due to Beer-Lambert's absorption and pH dependency of extinction coefficient, as shown in figure 11 a. Even if the ratiometric technique intrinsically corrects all inhomogeneities linked to excitation intensity, variations, introduced by the optical setup used to collect fluorescence, remain. As shown in figure 11 b, a spatial gradient of ratio, mostly horizontal, is introduced by these optical distortion and still has to be accounted for.

For that purpose, each calibration ratio field recorded is normalized by a reference ratio field taken at any pH.

$$R_n(M, pH) = \frac{R(M, pH)}{R_{ref}(M, pH_{ref})} \quad (16)$$

Where  $R_n$  is the normalized ratio which should not depend on  $M$ , and  $R_{ref}$  is the raw ratio field measured at reference  $pH_{ref}$ .

Applying such correction, the normalized ratio images become homogeneous (figure 11 c). The same normalization step is then applied to measurement images. In what follows, the normalized ratio  $R_n$  is called  $R$  for simplicity.

The experimental ratio as a function of pH is plotted in figure 12. The hyperbolic trend predicted

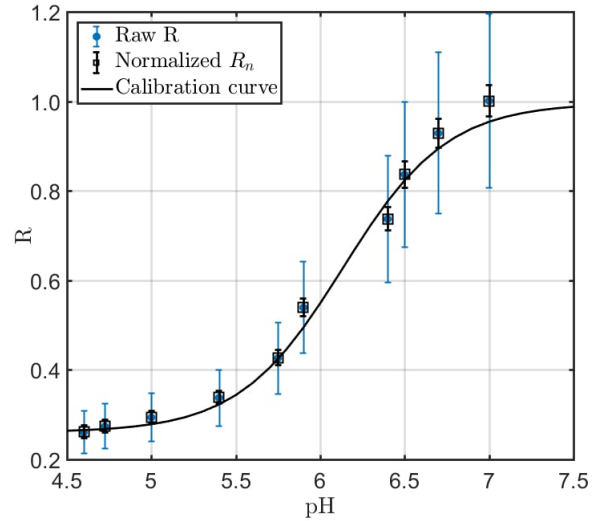


Fig. 12: Measured ratio as a function of pH

by the spectral study is found, which confirms that  $R = f(pH)$  calibration curve can be used for pH measurements. The error on the ratio, computed as the root mean square of the ratio values on the whole field, is of about 20 % (blue vertical bars) for raw fields due to the spatial heterogeneity, and falls to below 5 % (black vertical bars) for normalized ratio fields, as shown by the error bars of figure 12. This error is no longer due to an heterogeneous distribution but rather

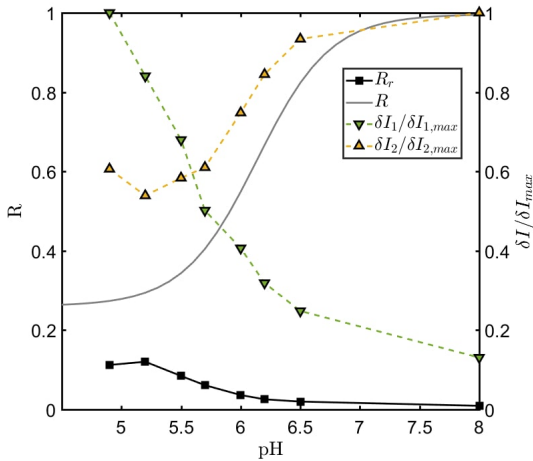


Fig. 13: Effect of fluorescence re-absorption on spectral band intensities and Ratio. Full line: Experimental curve for ratio without re-absorption  $R$  (figure 12), triangles: normalized intensity collected from band 1 (down-pointing) and 2 (up-pointing), squares:  $R_r$  ratio with re-absorption

to a random noise of pixel intensity values.

Finally, the impact of fluorescence re-absorption on fluorescence ratio can be illustrated by performing a calibration in similar optical setup but using a much higher fluorescein concentration, for example  $C = 3.1 \cdot 10^{-5} M$ . The path length of fluorescence towards the sensor is  $L_{obs} = 13.5 cm$  which gives  $C\epsilon L_{obs} \simeq 0.07$  for  $C = 5 \cdot 10^{-7} M$  at  $pH = 7$  and  $C\epsilon L_{obs} \simeq 4.22$  for the higher concentration, same pH. This last case should therefore be ascribed to re-absorption phenomena and the type III spectral conflict may become important.

In figure 13, it appears that  $R_r$  does not follow the same monotonic increasing trend when fluorescence re-absorption occurs. On the contrary the ratio tends to decrease with increasing pH (squares). A first approach explanation of this phenomenon can be proposed: since spectral band 1 is closer to the absorption domain than band 2, it is the one of the two bands that is the most sensitive to re-absorption (down-pointing triangles). As extinction coefficient  $\epsilon$  increases with the pH for all wavelengths, the proportion of band 1 fluorescence being reabsorbed also does. On the other hand, band 2's overlapping region with the absorption spectrum is much smaller than that of band 1, and so it is less prone to fluorescence re-absorption (up-pointing triangles). The pH increase still leads to increasing fluoresced intensity. Combining the two band's behaviors, the ratio decreases with increasing pH.

It seems clear that for cases where re-absorption and spectral conflict can not be avoided, i.e. when either the re-absorption path or dye concentration are large enough, the technique can not be used as it is presented here, and the use of a further correction procedure is required.

### 4.3 Results and interpretations

#### 4.3.1 Comparison of $I_{pH} - PLIF$ and $I_{pH}^r - PLIF$

In this paragraph, the results obtained by  $I_{pH}^r - PLIF$  are compared to those calculated by  $I_{pH} - PLIF$  using spectral band 1 only. Two calibration procedures are used for the single color approach. The one proposed by Souzy (2014), that is to say a pixel-by-pixel treatment accounting for extinction coefficient variations and where the curve for intensity as a function of pH is fitted by a 5<sup>th</sup> degree polynomial, and the common reference image normalization.

Before going any further, it has to be noted that the time needed to read, calibrate, and process a single image is at least 10 times longer for the pixel-by-pixel single color technique (typically 40 min with a common desktop computer) than for the simple normalization one color technique or the two-color one (4 min for calibration, less than 0.5 s for one image processing). This comes from the fact that each pixel has to be individually calibrated and treated for the first case, whereas a single fitting step is required in other cases. This time difference increases with the image resolution and the degree used for polynomial fitting of intensity curves.

Three instantaneous concentration fields are compared in figure 14. The scalar field obtained using the ratiometric technique appears to be less noisy than both single color version. Most of the "excitation noise" is corrected. For example, darker stripes due to the tank's wall scratches visible in figure 14 a and b, at the bottom right corner, almost completely disappear in figure 14 c. This tends to show that the two-color version is as expected more efficient when one has to deal with noisy excitation signal and reflections.

This feature is even better illustrated at the top of the figure, near the source of the jet. Here, unsteady reflections have been artificially introduced by making the free surface close to the jet oscillate. Such time dependent perturbations are still visible in figure 14 b and disappear on c.

One last interesting feature to be illustrated is the effect of unsteady laser output power (or intensity) hereinafter called power drift. For the two-color method

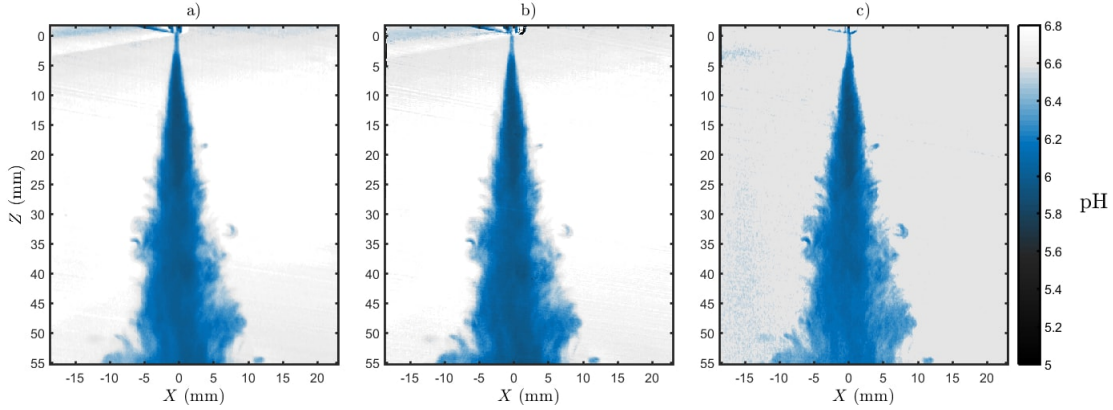


Fig. 14: Comparison of instantaneous pH field obtained by  $I_{pH} - PLIF$  using standard normalization (a) and pixel-by-pixel calibration (b), or by  $I_{pH}^r - PLIF$  (c)

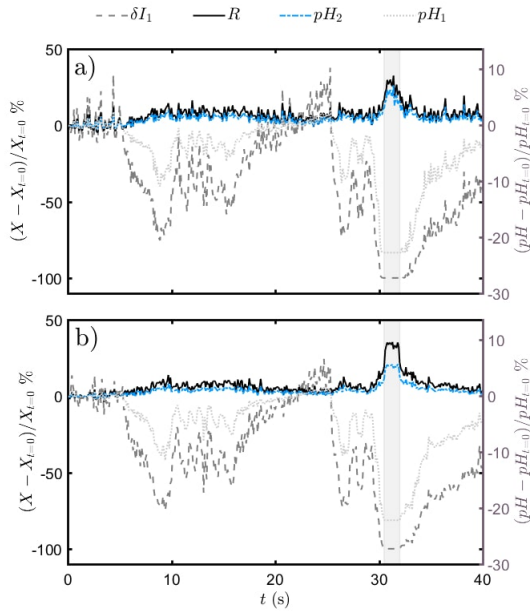


Fig. 15: Relative variations of band 1 intensity ratio and pH computed using single or two-color technique, in the bulk (a) and inside the jet (b) when applying a random laser power drift. Relative variations of  $\delta I_1$  and  $R$  are indicated on the left vertical axis and relative variations of  $pH_1$  and  $pH_2$  on the right vertical axis.

indeed, the laser power has no influence on the ratio, and so the power drift should be intrinsically corrected, providing that the power level remains sufficient for the two band's intensities to be measured with reasonable uncertainty.

In figure 15 are plotted time series of  $\delta I_1$  and  $R$  along with the corresponding pHs obtained by a one or two-color procedure, respectively denoted  $pH_1$  and

$pH_2$ . All quantities are measured at two points, one reference point in the bulk above the jet nozzle (figure 15 a) and one point inside the jet (figure 15 b). A random evolution of laser power input is imposed and leads directly to strong variations of  $\delta I_1$ . As expected, this induces an important error on the one color computed pH. For example, when  $\delta I_1$  is decreased by 50 %,  $pH_1$  is underestimated by about 7 % at point a and b. The ratio however remains almost constant with time in the bulk, and also inside the jet where most of its variations are not correlated to the variations of  $\delta I_1$  and correspond to turbulent pH fluctuations.  $pH_2$  consequently remains unchanged by the power drift.

Only at times between  $t = 30$  s and  $t = 35$  s appears an important ratio and  $pH_2$  variation at both points, reaching a plateau value between  $t = 31$  s and  $t = 32$  s. This corresponds to a case where the laser power output is such that the fluorescence signal is too low to be measured, especially at acidic pH where it falls of 100 %, i.e no more fluorescence coming from band 1 is measured either inside (b) or outside the jet (a). Ratio and pH computation from such low fluorescence signal is highly uncertain and can lead to large errors on  $pH_2$ . It still requires the power drift to be really strong for the ratiometric method to be laser power dependent.

#### 4.3.2 Jet characteristics

$I_{pH}^r - PLIF$  measurements are finally used to describe the jet characteristics. pH fields are converted into concentration using the equation  $pH = -\log(C_A)$ . Images at a  $f_r = 10$  Hz recording rate are collected and used to obtain average and RMS concentration. For the jet Reynolds number considered, the integral timescale of turbulence is about  $\tau_L = 320$   $\mu s$ , much smaller than the time between two frames, hence successive recorded im-

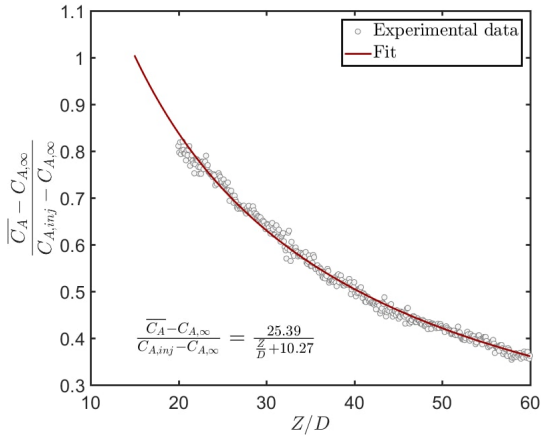


Fig. 16: Evolution of acid concentration along the jet centerline

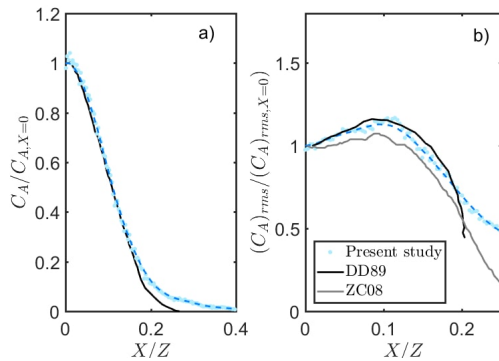


Fig. 17: Transverse profiles of averaged (a) and RMS (b) concentration for  $Z/D = 30$ , normalized by their respective values at  $X = 0$ . Present study is compared to the results of Dahm and Dimotakis (1987) (DD87) and Zarruk and Cowen (2008) (ZC08). DD87:  $Z/D = 300$ ,  $Re = 5000$ ; ZC08:  $63 < Z/D < 77$ ,  $Re = 4000$

ages are not statistically correlated. It is checked that 500 images are enough to reach statistical convergence of average and RMS fields.

Figure 16 shows the scaled acid concentration evolution along the jet centerline. The usual hyperbolic decaying law for passive scalar concentration is found for the range between 20 and 60 nozzle diameters (Chaze et al 2016; Papanicolaou and List 1988; Papantoniou and List 1989; Zarruk and Cowen 2008).

Transverse concentration profiles are shown in figure 17. The mean (a) and RMS (b) concentration profiles at  $Z/D = 30$  are scaled by their values at the centerline of the jet, and the jet width is normalized by the profile's distance to the nozzle.

The scaled mean concentration profile in figure 17 a corresponds to the results found by Dahm and Di-

motakis (1987) (DD87). As for RMS profiles in figure 17 b, it presents the expected shape with a peak value around  $X/Z = 0.1$ . Nevertheless, considering that it is taken closer to the nozzle ( $Z/D = 30$  versus  $Z/D > 60$ ) and for a lower Reynolds than for Dahm and Dimotakis (1987) or Zarruk and Cowen (2008) (ZC08), it should stay under both DD87 and ZC08 curves.

With the presented experimental design, accuracy of the result is not guaranteed for large  $Z/D$ , mainly due to an insufficient illumination leading to a poor signal to noise ratio in the far jet region. The current setup was meant to perform a proof of concept of  $I_{pH}^r - PLIF$ . An in depth jet study would require to adapt it and enlarge the region of interest to  $Z/D$  values where an effective measurement of RMS concentration profiles could be done.

## 5 Discussion and conclusions

In this work, the interest of the original  $I_{pH}^r - PLIF$  technique has been demonstrated. The ratio of intensities from two well chosen spectral bands of fluorescein's fluorescence spectrum increases with the pH, with a good dynamics in the range between pH 5 and 7. This behavior comes from the wavelength-variable pH dependency of fluorescein's quantum yield. It can be used to translate two recorded fluorescence fields into a quantitative pH field thanks to an initial calibration procedure, in a similar way to what is currently done for temperature measurements. The use of a single dye lowers the potential chemical intrusiveness of the technique, and makes it more suitable for the study of turbulent flows than two dyes versions.

Two limitations are still to be mentioned. First of all, the overlapping between fluorescein's absorption and emission spectra leads to an unsolvable form of spectral conflict. This conflict can cause fluorescence re-absorption if the path crossed by fluoresced light is long, or if the dye concentration level is too important. It can therefore introduce large errors on the measured ratio, hence on the computed pH fields.

Second is the fact that fluorescence recording on sCMOS sensors requires a rather long exposure time, typically of 20 ms in the present study. This is especially due to the fact that since a single dye is used, at least one of the two-color emits a relatively low fluorescence signal. Thus, a longer exposure time is needed for a significant signal from this color to be recorded. It implies that the faster scales of turbulence can not be captured. To decrease this exposure time, more powerful continuous light sources or pulsed lasers can be used to increase the excitation intensity. Fluctuations of emitted intensity output known to occur for pulsed

lasers are automatically corrected by the use of ratio-metric technique in a way similar to power drift corrections presented in section 4.3.1 (Bruchhausen et al (2005)). However, increasing the laser output intensity may generate excitation intensities above the linear domain limit (Chaze et al (2016)), or introduce photo-bleaching effects. Furthermore, pulsed laser are difficult to find for the present excitation wavelength, and generation of pulses from continuous laser at this wavelength adds supplementary difficulties.

To conclude,  $I_{pH}^r - PLIF$  presents two main assets:

- It can be applied anywhere in the flow, even on small regions, regardless of the incident light absorption conditions outside the region of interest. Indeed, the knowledge of the laser path across the fluid and the pH variation it may encounter on its way to the ROI is not required. This makes the technique interesting for studying small scale or local phenomena, or for accessing specific regions of complex flows.
- It intrinsically corrects several errors that can't be accounted for by single color techniques, such as time variations of excitation intensity or reflections at moving interfaces. Recently, Chaze et al (2017) have successfully measured temperature fields in droplets impinging of solid surfaces using two dyes ratiometric LIF measurements. This last point in particular offers interesting perspectives for  $I_{pH}^r - PLIF$  applications in multiphase mass transfer studies.

**Acknowledgements** The authors gratefully thank Jean-Marie Bluet and the INL laboratory for providing the spectrofluorimeter used for the fluorescence studies.

## References

- Asher WE, Litchendorf TM (2008) Visualizing near-surface concentration fluctuations using laser-induced fluorescence. *Experiments in Fluids* 46(2):243–253
- Bassnett S, Reinisch L, Beebe DC (1990) Intracellular pH measurement using single excitation-dual emission fluorescence ratios. *American Journal of Physiology - Cell Physiology* 258(1):C171–C178
- Bruchhausen M, Guillard F, Lemoine F (2005) Instantaneous measurement of two-dimensional temperature distributions by means of two-color planar laser induced fluorescence (PLIF). *Experiments in Fluids* 38(1):123–131
- Brujan E (2010) *Cavitation in Non-Newtonian Fluids: With Biomedical and Bioengineering Applications*. Springer Science & Business Media
- Buckler KJ, Vaughan-Jones RD (1990) Application of a new pH-sensitive fluoroprobe (carboxy-SNARF-1) for intracellular pH measurement in small, isolated cells. *Pflügers Archiv* 417(2):234–239
- Butler C, Cid E, Billet AM (2016) Modelling of mass transfer in Taylor flow: Investigation with the PLIF-I technique. *Chemical Engineering Research and Design* 0(0)
- Chaze W, Caballina O, Castanet G, Lemoine F (2016) The saturation of the fluorescence and its consequences for laser-induced fluorescence thermometry in liquid flows. *Experiments in Fluids* 57(4):58
- Chaze W, Caballina O, Castanet G, Lemoine F (2017) Spatially and temporally resolved measurements of the temperature inside droplets impinging on a hot solid surface. *Experiments in Fluids* 58(8):96
- Coolen MCJ, Kieft RN, Rindt CCM, Steenhoven AAV (1999) Application of 2-D LIF temperature measurements in water using a Nd : YAG laser. *Experiments in Fluids* 27(5):420–426
- Coppeta J, Rogers C (1998) Dual emission laser induced fluorescence for direct planar scalar behavior measurements. *Experiments in Fluids* 25(1):1–15
- Crimaldi JP (2008) Planar laser induced fluorescence in aqueous flows. *Experiments in Fluids* 44(6):851–863
- Dahm WJA, Dimotakis PE (1987) Measurements of entrainment and mixing in turbulent jets. *AIAA Journal* 25(9):1216–1223
- Doughty MJ (2014) Fluorescence characteristics of sodium fluorescein–rose bengal ophthalmic solution mixtures. *Contact Lens and Anterior Eye* 37(5):358–362
- Guilbault GG (1990) *Practical Fluorescence*, Second Edition. CRC Press
- Jimenez M (2013) *Etude du transfert de matière gaz/liquide en milieux complexes : quantification du transfert d'oxygène par techniques optiques*. PhD thesis, Toulouse, INSA
- Kawase Y, Halard B, Moo-Young M (1987) Theoretical prediction of volumetric mass transfer coefficients in bubble columns for Newtonian and non-Newtonian fluids. *Chemical Engineering Science* 42(7):1609–1617
- Klonis N, Sawyer WH (1996) Spectral properties of the prototropic forms of fluorescein in aqueous solution. *Journal of Fluorescence* 6(3):147–157
- Kováts P, Thévenin D, Zähringer K (2017) Characterizing fluid dynamics in a bubble column aimed for the determination of reactive mass transfer. *Heat and Mass Transfer* pp 1–9
- Kuhn S, Jensen KF (2012) A pH-Sensitive Laser-Induced Fluorescence Technique To Monitor Mass Transfer in Multiphase Flows in Microfluidic De-

- vices. *Industrial & Engineering Chemistry Research* 51(26):8999–9006
- Lacassagne T, EL Hajem M, Morge F, Simoens S, Champagne JY (2017) Study of Gas Liquid Mass Transfer in a Grid Stirred Tank. *Oil & Gas Science and Technology – Revue d'IFP Energies nouvelles* 72(1):7
- Lavielle P, Delconte A, Blondel D, Lebouché M, Lemoine F (2004) Non-intrusive temperature measurements using three-color laser-induced fluorescence. *Experiments in Fluids* 36(5):706–716
- Lehwald A, Thévenin D, Zähringer K (2010) Quantifying macro-mixing and micro-mixing in a static mixer using two-tracer laser-induced fluorescence. *Experiments in Fluids* 48(5):823–836
- Lindqvist L (1960) A flash photolysis study of fluorescein. *Almqvist & Wiksell*
- Martin MM, Lindqvist L (1975) The pH dependence of fluorescein fluorescence. *Journal of Luminescence* 10(6):381–390
- Morris S (1990) Real-time multi-wavelength fluorescence imaging of living cells. *BioTechniques* 8(3):296–308
- Natrajan VK, Christensen KT (2009) Two-color laser-induced fluorescent thermometry for microfluidic systems. *Measurement Science and Technology* 20(1):015,401
- Papanicolaou PN, List EJ (1988) Investigations of round vertical turbulent buoyant jets. *Journal of Fluid Mechanics* 195:341–391
- Papantoniou D, List EJ (1989) Large-scale structure in the far field of buoyant jets. *Journal of Fluid Mechanics* 209:151–190
- Roudet M, Billet AM, Cazin S, Risso F, Roig V (2017) Experimental investigation of interfacial mass transfer mechanisms for a confined high-reynolds-number bubble rising in a thin gap. *AIChE Journal* 63(6):2394–2408
- Sakakibara J, Adrian RJ (1999) Whole field measurement of temperature in water using two-color laser induced fluorescence. *Experiments in Fluids* 26(1-2):7–15
- Sakakibara J, Hishida K, Maeda M (1997) Vortex structure and heat transfer in the stagnation region of an impinging plane jet (simultaneous measurements of velocity and temperature fields by digital particle image velocimetry and laser-induced fluorescence). *International Journal of Heat and Mass Transfer* 40(13):3163–3176
- Simoens S, Ayrault M (1994) Concentration flux measurements of a scalar quantity in turbulent flows. *Experiments in Fluids* 16(3-4):273–281
- Sossa-Echeverria J, Taghipour F (2012) Mixing of Newtonian and Non-Newtonian Fluids in a Cylindrical Mixer Equipped with a Side-Entry Impeller. *Industrial & Engineering Chemistry Research* 51(46):15,258–15,267
- Souzy N (2014) Experimental study and improvement of mass transfer in vertical bubble columns. phdthesis, Université Claude Bernard - Lyon I
- Stumm W, Morgan JJ (1996) *Aquatic chemistry: chemical equilibria and rates in natural waters*. Wiley
- Turney DE, Banerjee S (2013) Air–water gas transfer and near-surface motions. *Journal of Fluid Mechanics* 733:588–624
- Valiorgue P, Souzy N, El Hajem M, Ben Hadid H, Simoëns S (2013) Concentration measurement in the wake of a free rising bubble using planar laser-induced fluorescence (PLIF) with a calibration taking into account fluorescence extinction variations. *Experiments in Fluids* 54(4):1–10
- Valiorgue P, Ben Hadid H, El Hajem M, Rimbaud L, Muller-Feuga A, Champagne JY (2014) CO<sub>2</sub> mass transfer and conversion to biomass in a horizontal gas–liquid photobioreactor. *Chemical Engineering Research and Design* 92(10):1891–1897
- Variano EA, Cowen EA (2013) Turbulent transport of a high-Schmidt-number scalar near an air–water interface. *Journal of Fluid Mechanics* 731:259–287
- Walker DA (1987) A fluorescence technique for measurement of concentration in mixing liquids. *Journal of Physics E: Scientific Instruments* 20(2):217
- Xu F, Jimenez M, Dietrich N, Hébrard G (2017) Fast determination of gas-liquid diffusion coefficient by an innovative double approach. *Chemical Engineering Science* 170:68–76
- Zarruk GA, Cowen EA (2008) Simultaneous velocity and passive scalar concentration measurements in low Reynolds number neutrally buoyant turbulent round jets. *Experiments in Fluids* 44(6):865–872